Applied Geochemistry 140 (2022) 105285

Contents lists available at ScienceDirect

Applied Geochemistry

journal homepage: www.elsevier.com/locate/apgeochem

Rate and capacity of cation release from ultramafic mine tailings for carbon capture and storage

Xueya Lu *, Kate J. Carroll, Connor C. Turvey, Gregory M. Dipple

Carbmin Lab, Department of Earth, Ocean and Atmospheric Sciences, The University of British Columbia, 2020 – 2207 Main Mall, Vancouver, BC, V6T 1Z4, Canada

ARTICLE INFO

Editorial handling by Dr D. Wolff-Boenisch

Keywords:
Mineral carbonation
Reactivity
Transient dissolution
Mineral dissolution kinetics
Labile cations
Labile Mg
Ultramafic mine tailings

ABSTRACT

Solid wastes produced during hard-rock mining have capacity to capture and store atmospheric CO_2 via dissolution and precipitation of Mg-bearing carbonate minerals. However, there is a discrepancy in our understanding of weathering and dissolution in these wastes, with dissolution and reaction rates in field studies exceeding those predicted by experiments under far-from-equilibrium conditions. To reconcile these differences, a series of flow-through dissolution experiments at 25 °C and 1atm were performed to investigate the short-term dissolution kinetics of ultramafic tailings and minerals. Results show that mineral and tailings samples have two stages of dissolution: a fast, transient (or labile) stage, and a slow, stoichiometric stage. Fast releasing labile cations (i.e. labile Mg^{2+}) are sourced from trace minerals with a high reaction rate (e.g. brucite) and from non-stoichiometric surface reaction processes of major minerals (e.g. serpentine). These cations are missing from most geochemical models for mineral weathering. The implication of these results is that the initial transient dissolution of minerals, which is typically ignored during geochemical investigations into bulk dissolution rates, is the missing ingredient for understanding dissolution of mine tailings. Labile cations released during the initial transient dissolution process have value for rapid and low-cost carbon capture and storage techniques as they represent reactivity, capacity, and the best opportunities to deploy low-cost carbon sequestration techniques using mine tailings and other industrial wastes. The presence of labile cations and changing reaction rates over time may also suggest that short-term reactivity examined during field tests may overestimate long-term carbon capture potential of some sites.

1. Introduction

The continuous rise in anthropogenic CO_2 levels is significantly disturbing the global carbon cycle and leading to global climate change (IPCC, 2018 and IPCC, 2021). Mineral carbonation, also known as carbon mineralization, is one of the many strategies that has been proposed and investigated to capture, store and utilize the excess CO_2 in the atmosphere (Seifritz, 1990; Gerdemann et al., 2007; Oelkers et al., 2008; Pronost et al., 2011; Harrison et al., 2013; Power et al., 2013; Gislason et al., 2014; Hellevang, 2015; McGrail et al., 2016; Razot et al., 2019; Hills et al., 2020). This process first involves the liberation of metal cations (such as Ca^{2+}, Fe^{2+} and Mg^{2+}) from minerals via dissolution or surface-ion exchange processes. The second step is the introduction of CO_2 and the subsequent precipitation of carbonate minerals with the liberated divalent metal cations. Mineral carbonation can use a variety of materials as feedstocks, including mafic and ultramafic rocks and mine tailings (Power et al., 2013; Kandji et al., 2017a, 2017b; Ruggieri and Gherardi., 2020; Eloneva et al., 2008; Han et al., 2015; Liu et al., 2018), and industrial wastes such as steel and blast furnace slag. Through mineral carbonation, CO_2 is stored permanently as environmentally benign and stable carbonate minerals, reducing the need for post storage monitoring. One of the challenges associated with mineral carbonation is that reaction kinetics need to be accelerated to sequester meaningful amounts of CO_2 within the necessary time frame to reduce the impact of climate change. Proposed strategies to accelerate the carbonation of ultramafic tailings include the use of elevated temperature and pressure to accelerate carbonation reaction rates (Sipilä et al., 2008; Béarat et al., 2006; Kelemen and Matter, 2008; Zevenhoven et al., 2008; Koukouzas et al., 2009; Krevor and Lackner, 2011; Fagerlund et al., 2012; Wang et al., 2019). However, the substantial energy consumption and financial costs make them work-intensive and less carbon-friendly, limiting their viability.

Recent research has been directed toward improving the efficiency of mineral dissolution under ambient conditions (Arce et al., 2017). These

* Corresponding author.
E-mail address: xlu@eoas.ubc.ca (X. Lu).

https://doi.org/10.1016/j.apgeochem.2022.105285
Received 17 January 2022; Received in revised form 20 March 2022; Accepted 22 March 2022
Available online 25 March 2022

Table 1
Geochemical composition of samples determined by X-ray fluorescence spectroscopy.

Sample ID	SiO_2	Al_2O_3	Fe_2O_3	CaO	MgO	Na_2O	K_2O	
	wt%	wt%	wt%	wt%	wt%	wt%	wt%	
BrQtz mix	89.64	0.29	0.16	0.19	5.58	<0.01	0.07	
Serpentine	38.80	0.58	7.46	0.35	37.84	0.05	0.12	
Forsterite	31.81	0.16	8.41	0.03	58.99	0.23	0.04	
GK1	38.74	3.57	7.46	7.24	28.77	0.59	1.29	
BD1	34.26	0.16	9.63	0.02	41.92	0.07	<0.01	
BD2	38.15	1.36	4.11	0.57	43.19	0.15	0.04	
MKM	33.42	0.14	5.03	0.17	46.77	0.17	0.02	
Sample ID	**Cr_2O_3**	**TiO_2**	**MnO**	**P_2O_5**	**SrO**	**BaO**	**L.O.I.**	**Total**
	wt%	wt%	wt%	wt%	wt%	wt%	wt%	wt%
BrQtz mix	<0.01	0.02	0.01	0.01	<0.01	<0.01	3.82	99.8
Serpentine	0.24	0.04	0.1	0.02	<0.01	0.01	13.38	99.0
Forsterite	0.18	0.01	0.12	0.02	<0.01	0.01	<0.01	100.0
GK1	0.22	0.63	0.13	0.23	0.04	0.10	10.65	99.6
BD1	0.55	<0.01	0.11	0.002	<0.01	<0.01	12.9	99.6
BD2	0.24	0.03	0.1	0.02	<0.01	0.01	12.13	100.1
MKM	0.18	0.01	0.08	0.02	<0.01	0.01	13.5	99.5

approaches utilize the reactivity of the materials while maximizing the economic feasibility at the industrial scale. Many studies have demonstrated that mineral carbonation occurs passively in alkaline wastes generated from the mining of ultramafic rocks at many mine sites worldwide (Power et al., 2009; Wilson et al., 2014; Lechat et al., 2016; Beaudoin et al., 2017). At the Mount Keith nickel mine (Western Australia, Australia) and the Diavik diamond mine (Northwest Territories, Canada), atmospheric CO_2 is sequestered at 40,000t CO_2 $year^{-1}$ and 400t CO_2 $year^{-1}$ respectively (Wilson et al., 2009, 2014). Mineral carbonation occurs in tailings at accelerated rates because industrial milling processes decrease grain size and increase surface areas, thereby promoting dissolution kinetics (Vance et al., 2009; Vogeli et al., 2011; Lechat et al., 2016; Miller and Naeth, 2017; Bullock et al., 2021). Mineral dissolution rates under ambient conditions are often slow, and the extent of reactions is limited; however, there is substantial variability between and within individual deposits due to the heterogeneity in mineral variability and the reactivity of individual mineral phases (Murphy and Helgeson, 1987; Aoba et al., 1992; Assima et al., 2012; Daval et al., 2013; Razote et al., 2019; Paulo et al., 2021; Tutolo et al., 2021; Woodall et al., 2021).

Conventional mineral dissolution studies have focused on determining long-term the steady-state dissolution kinetics of specific minerals using laboratory experiments under a variety of conditions. The effect of pH, temperature, and pressure (Vermilyea, 1969; Mellini, 1982; Jordan and Rammensee, 1996; Stumm, 1997; Metz and Ganor, 2001; Pokrovsky and Schott, 2000; 2004; Amram and Ganor, 2005; Daval et al., 2013; Harrison et al., 2013; Lechat et al., 2016) and the presence ligands (Zinder et al., 1986; Stumm et al., 1987; Bondietti et al., 1993; Pokrovsky et al., 2005; Cama and Ganor, 2006) on the weathering kinetics of common minerals in ultramafic mine tailings such as brucite [$Mg(OH_2)$], serpentine [$Mg_3Si_2O_5(OH)_4$], forsterite (Mg_2SiO_4) and hydrotalcite group minerals [eg. pyroaurite, $Mg_6Fe^{3+}{}_2(CO_3)(OH)_{16}\bullet 4(H_2O)$] have been studied (Seyama et al., 1996; Mills et al., 2012; De Baere et al., 2015; Melchiorre et al., 2017; Oelkers et al., 2018; Turvey et al., 2018). These experiments have provided a wealth of data on the rate and dissolution mechanisms under various experimental conditions. Mg-hydroxide minerals, such as brucite, can undergo complete dissolution within a short period due to their relatively reactive crystal structure and composition (Azizi and Larachi, 2019). In contrast, the dissolution of Mg-silicates is much slower.

While conventional mineral dissolution studies provide a wealth of information on the kinetics of various minerals, there is a discrepancy between dissolution rates seen in the laboratory and weathering rates observed in the field, with weathering rates often exceeding those predicted by laboratory studies (Matter et al., 2009; Ragnheidardottir et al., 2011; Gislason et al., 2014; Snæbjörnsdóttir et al., 2018; Beerling et al., 2018, 2020). As mineral carbonation reactions rely on the amount of labile cations produced *in-situ*, understanding this discrepancy could enable better predictions of mineral carbonation potential in a given mine site. Prior to now, many laboratory dissolution studies have demonstrated transient, non-stoichiometric silicate mineral dissolution prior to long-term steady-state dissolution (Luce et al., 1972; Stumm, 1987; Wieland & Stumm., 1992; De Baere et al., 2015). However, very little attention was devoted to understanding these early stages of dissolution and determining how these transient rates vary with mineralogy, acid strength and dissolution mechanism as they were not representative of bulk dissolution processes. In fact, this early transient dissolution could represent the missing reactivity necessary to align the laboratory dissolution rates and weathering rates observed in the field.

This study examines the dissolution behaviour of typical ultramafic tailings and minerals under various chemical and pH conditions, focusing on reaction rates during the early stages of dissolution. Samples were analyzed using a flow-through dissolution reactor to better observe far from equilibrium conditions and monitor changing environmental conditions over time. Reaction rates, cumulative Mg^{2+} leached, and reaction time is used to evaluate the mineral carbonation reactivity of individual mineral phases and ultramafic tailings. By improving the understanding of this early-stage dissolution, we can guide ongoing mineral carbonation research and offer an accurate evaluation of the total mineral carbonation reactivity within mine tailings.

2. Materials and methods

2.1. Sample preparation and characterization

Nine samples were analyzed in this study, including four ultramafic tailings and four pure mineral phases, brucite, serpentine, quartz, forsterite and a synthetic compound with the composition and structure of pyroaurite. High purity pulverized brucite ore was sourced from Brucite Mine (Gabbs District, Nevada, USA). The brucite sample used during dissolution experiments was prepared as a brucite-quartz mixture by mechanically mixing 10 wt% high-purity brucite ore with 90 wt% quartz sand. Brucite-quartz mix is used to decrease the sample size of brucite so that complete dissolution can be achieved within the expected experimental duration. Serpentine samples were obtained from the Swift Creek landslide in northwest Washington (USA). The serpentine is a fresh sample that was not heat treated or chemically altered. Natural quartz sand was sourced from Lane Mountain Company (Washington, USA). Ward's Natural Science supplied forsterite grains from the Twin Sisters dunite (Washington, USA) (item#: 470025-722). The artificial sample of

Table 2
Summary of important XRD mineral abundances and BET surface area values.

	10Br90Qtz	Serpentine (Lizardite)	Forsterite	Hydrotalcite (Pyroaurite)	GK1	BD1	BD2	MKM
Serpentine (wt%)[a]	0.4	91.9			47.4	81.1	93.8	78.3
Brucite (wt%)[b]	8.9				0.1	8.9	1.7	5.9
Diopside (wt%)[a]			–		3.4		2.3	
Pyroaurite (wt%)[b]				100.0				8.1
Forsterite (wt%)[a]		–	94.9		–	3.8	2.3	
Magnesite (wt%)[a]	0.5				–	–		2.8
Phlogopite (wt%)[a]	2.2	3.6			18.3	–		
BET Surface Area (m^2g^{-1})	0.53	18.5	0.23	66.1	9.36	3.84	10.8	2.5

[a] Abundance determined by qXRD.
[b] Abundance determined by TGA.

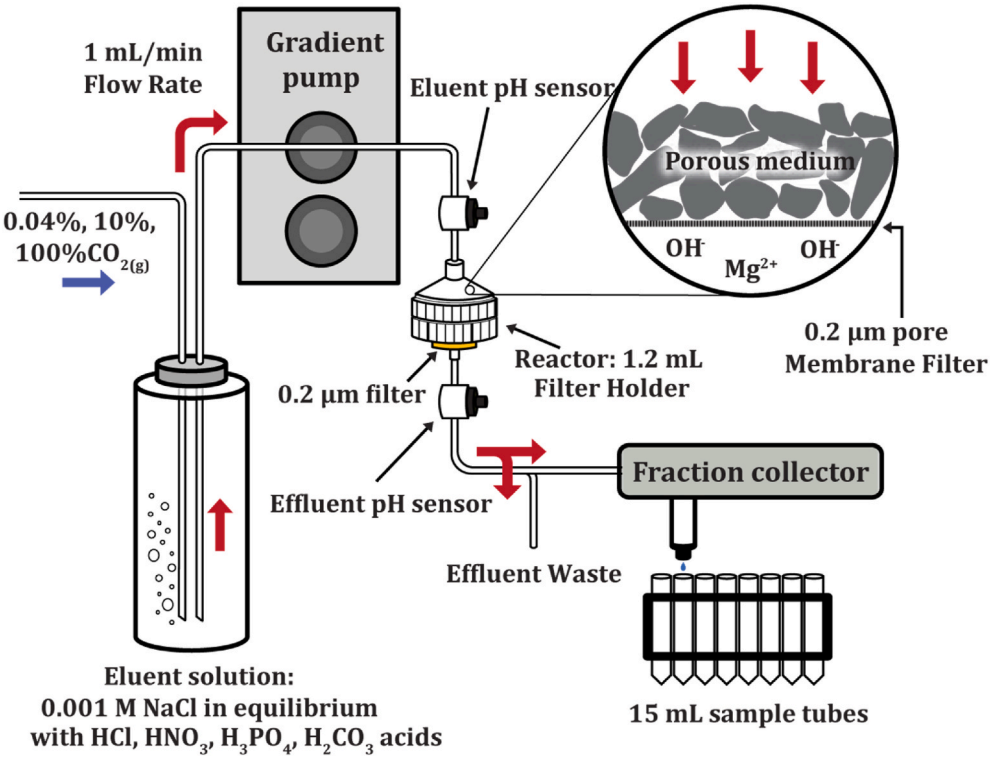

Fig. 1. Schematic diagram of the flow-through time-resolved analysis (FT-TRA) experimental apparatus.

pyroaurite was produced by the direct synthesis in the lab; detailed methods are described in Turvey (2018) based on a modified version of the Vucelic et al. (1997) method. Of the four ultramafic tailings samples, two are simulated nickel tailings from the Decar nickel district in central British Columbia, Canada (BD1 and BD2), and one is from the Mount Keith nickel mine in Western Australia (MKM). A fourth tailings sample is processed kimberlite from the Gaucho Kué Mine in Northwest Territories, Canada (GK1). Desired size fractions (53–106 µm) of all samples were obtained by dry-milling and dry screening. All samples were then ultrasonically cleaned using pure ethanol to remove fine particles rinsed with reverse osmosis water (resistivity ≥15 MΩ cm) for 5 min before being air-dried at room temperature. The tailings samples were then sieved while suspended in deionized water (wet-sieved) to further remove fine particles before undergoing similar processing as the mineral samples.

All samples were characterized for their mineralogical composition (via quantitative X-ray diffraction (qXRD), thermogravimetric analysis (TGA), specific surface area [via multi-point Brunauer–Emmett–Teller (BET) method with N_2 gas absorption], and particle size distributions (via a Malvern Mastersizer 2000 laser diffraction particle-size analyzer). Major element oxide compositions of the starting materials were determined using X-ray fluorescence spectroscopy (XRF; Table 1) at ALS Global Laboratories, North Vancouver, British Columbia, using lithium borate fusion digestion. Brucite abundance in minerals and tailings samples is taken from values measured using Thermogravimetric analysis (TGA) because qXRD analysis typically results in a high relative error for minerals at low abundance (Raudsepp et al., 1999; Tosca and Masterson, 2014; Arce et al., 2017; Turvey et al., 2018). XRD abundance of other minerals was normalized to 100%, incorporating the TGA brucite estimate. The detailed analytical methodology and normalization calculations of XRD and TGA measurements can be found in Table S1.2, Supplementary Information (S.I.). The relevant sample characterization results are summarized in Table 2.

2.2. Flow-through dissolution experimental set-up

Flow-through dissolution experiments were conducted using a purpose-built flow-through time-resolved analysis (FT-TRA) module (Fig. 1). The design and the experimental protocol used in this study are a modification of the procedure used by De Baere et al. (2015). The experimental module included a Dionex ICS-3000 dual-gradient pump operating at a flow rate of 1.0 mL/min and a Foxy®R1 fraction collector

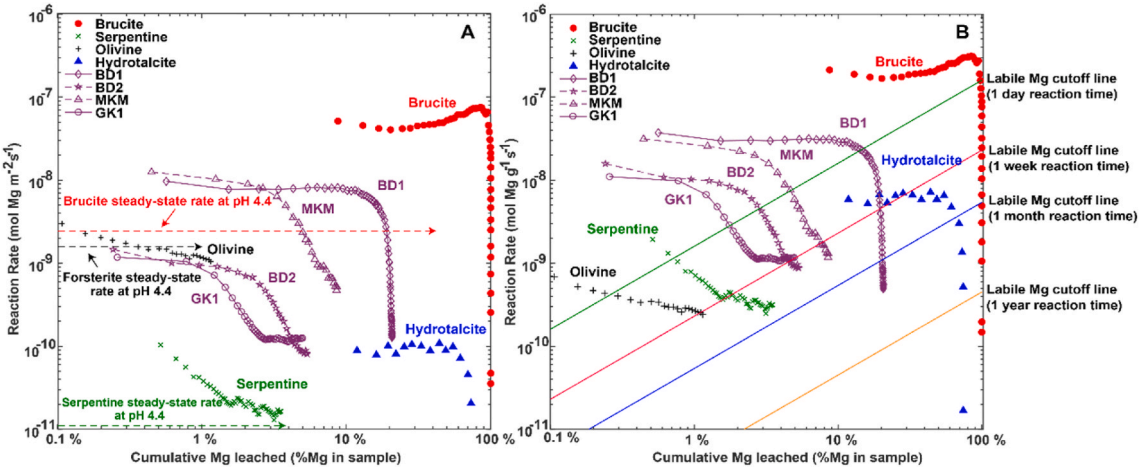

Fig. 2. Dissolution rates versus cumulative Mg leached for minerals and tailings samples at pH = 4.4, pCO_2 = 0.1 bar. (A) Dissolution rate normalized to BET surface area (mol Mg m^{-2} s^{-1}), steady-state dissolution rates of minerals from literature are plotted in coloured dashed lines. (B) Dissolution rate normalized to sample mass (mol Mg g^{-1} s^{-1}), labile Mg cut-off line at different residence times are plotted as coloured 1:1 ratio lines.

connected entirely with metal-free polyetheretherketone (PEEK) flow tubes. The reaction chamber was assembled using a 25 mm diameter polypropylene Swinnex filter holder (1.2 mL internal volume) containing a 0.2 μm polycarbonate membrane filter (Millipore catalogue #SLLGC13NL). Weighed sample aliquots were loaded into the sample holder and then shaken to distribute the sample evenly. The sample holder was mounted vertically between two parallel, remotely controlled solenoid valves and above a 0.2 μm syringe filter (diameter: 13 mm). The syringe filter provided secondary filtration to prevent fine particulates from clogging the PEEK tubes. Inlet solution (eluent) flowed through the top solenoid valve, the 1.2 mL reaction chamber, the membrane filter, and the lower solenoid valve. Polytetrafluoroethylene (PTFE) sealant tape was wrapped around the threading on the screw-fitting of the filter holder to prevent any potential leaks that could occur due to pressure build-up inside the reaction chamber. The dissolution experiments were performed at room temperature and pressure (21–25 °C, 1 atm). The experiment duration ranged between 70 and 120 h. The conditions of all experiments are summarized in Table S4.1 (see S.I.)

2.3. Fluid composition analysis and rate calculation

Four types of acids were used to prepare the inlet fluids (eluent) solutions used in this study: hydrochloric (HCl: 37% ACS Reagent Grade, Sigma-Aldrich Corporation), phosphoric (H_3PO_4: 85% ACS Reagent Grade, Sigma-Aldrich Corporation), nitric (HNO_3: 70%. Trace Metal Grade, Fisher Scientific International, Inc.) and carbonic (H_2CO_3). The carbonic acid was created by bubbling CO_2 gas of various concentrations through the 0.001M NaCl solution. The CO_2 varied between experiments with 0.04%, 10%, and 100% CO_2 concentrations. 10% CO_2 was chosen to approximate the CO_2 concentration of flue gas from the combustion of fossil fuel, while 0.04% CO_2 is the CO_2 concentration of air (Zevenhoven et al., 2008; Sanna et al., 2014; Songolzadeh et al., 2014). Compressed tank gas of 10% and 100% CO_2 were from Praxair Canada Inc, and 0.04% CO_2 was sourced from CO_2 in the ambient laboratory air. Carbonic acid solutions were equilibrated for a minimum of 24 h before the commencement of each experiment to ensure that pH stabilized near the expected value (pH = 5.60, pH = 4.41, pH = 3.89) based on PHREEQC (Parkhurst and Appelo, 2013) modelling. The CO_2 abundance converted in ppm, %, bar and equivalent pH value is reported in Table S1.1 (see S.I.). The outlet fluids (effluent), approximately 13 mL per sample, were collected at intervals ranging from 30 min to 2 h for the duration of the experiment. Fluid composition from each experiment was analyzed for Al, Ca, Fe, K, Mg, Na, and Si concentration using a Varian 725-ES inductively coupled plasma optical emission spectrometer (ICP-OES) at the University of British Columbia. The detection limit for measured elements is reported in Table S1.3 (see S.I). The post-experimental solid material was preserved, dried overnight, and weighed for qualitative XRD analysis.

The mineral dissolution rate was normalized to both the sample total surface area and to the sample mass in units of mol Mg m^{-2} s^{-1} and mol Mg g^{-1} s^{-1}. The mineral dissolution rate in mol Mg m^{-2} s^{-1} was calculated based on solution Mg concentration, mineral reactive surface area, and flow rate using Eq. (1) and Eq. (2) (adapted from Daval et al., 2013).

$$R_{Mg(molMgm^{-2}s^{-1})} = \frac{r_f \Delta_{[Mg]}}{\eta_{Mg} A_{BET} m_0} \quad (1)$$

$$R_{Mg(molMgg^{-1}s^{-1})} = \frac{r_f \Delta_{[Mg]}}{\eta_{Mg} m_0} \quad (2)$$

where R_{Mg} is the dissolution rate based on [Mg], r_f is the flow rate (L s^{-1}), $\Delta_{[Mg]}$ is the difference between the effluent and the eluent [Mg] (mol L^{-1}), η_{Mg} is the mineral stoichiometric coefficient of Mg, and m_0 is the initial mass of mineral reactant (g). A_{BET} (m^2 g^{-1}) is the reactive surface area measured using the BET method. The mineral dissolution rate in mol Mg g^{-1} s^{-1} (Eq. (2)) was calculated without considering the mineral surface area A_{BET} (m^2 g^{-1}).

3. Results & discussion

3.1. Labile cations and labile Mg

Results from the flow-through experiments show a wide variety of dissolution behaviour between different pure minerals and tailings samples. In Fig. 2, cumulative Mg^{2+} leached (%) is plotted against reaction rate normalized by mineral surface area (Fig. 2A) and sample weight (Fig. 2B), for all the mineral and tailings samples, under the same chemical conditions (pH = 4.4, pCO_2 = 0.1 bar). From Fig. 2, we see that the bulk dissolution rate of brucite in solution with 10%CO_2 is faster than that of the Mg-silicates (i.e. olivine and serpentine) and synthetic pyroaurite. It can also be observed that brucite, serpentine and forsterite dissolved faster than the steady-state rates determined in literature, especially near the beginning of the experiment (Vermilyea, 1969; Jordan and Rammensee, 1996; Pokrovsky & Schott, 2000, 2004; Palandri and Kharaka, 2004; Thom et al., 2013; Daval et al., 2013). Brucite is approximately 2 orders of magnitude faster while serpentine and olivine are around one order of magnitude and 3 times faster,

respectively, reasons for which will be explored in section below on labile Mg dependence on acid types and pCO_2. Finally, the rate of tailings dissolution falls in between that of the minerals (Fig. 2).

Brucite showed the fastest dissolution rate and furthest reaction extent of all the minerals reacting at a steady state of $\sim10^{-7}$ mol Mg g^{-1} s^{-1} until ~90% of the Mg has been leached from the sample, at which point the reaction rate rapidly falls (Fig. 2B). The decline in reaction rate is due to the consumption of reactive mineral grains approaching 100% reaction. The steady-state mineral dissolution rates (i.e. brucite, serpentine, olivine) from literature are renormalized using BET surface area measured in this study before making the comparison (Figs. 2 and 4) (see detailed discussion in S.I. section S3). The synthetic pyroaurite sample exhibited similar steady-state dissolution behaviour as the brucite, but at a lower rate of $\sim10^{-8}$ mol Mg g^{-1} s^{-1} until ~60% of the Mg has dissolved, after which the reaction rate rapidly falls. The Mg-silicates serpentine and olivine exhibited markedly different reaction behaviour to the brucite and pyroaurite with a 2-stage dissolution. Their initial transient reaction rates were relatively high ($\sim4.7\bullet10^{-10}$ mol Mg m^{-2} s^{-1} for serpentine, $\sim1.7\bullet10^{-8}$ mol Mg m^{-2} s^{-1} for olivine) but slowed over time, approaching a plateau at their steady-state literature dissolution rates ($\sim10^{-11}$ for serpentine, $\sim1.6\bullet10^{-9}$ for olivine) (Fig. 2A). In the case of olivine, it reached steady-state dissolution after 10 h, by which point it had leached ~0.5% of the total Mg in the sample, while serpentine had not yet reached steady-state after the experiment ended at 78 h, during which it had dissolved ~4% of the total Mg in the sample (Fig. 2B).

In Fig. 2, reaction rate were examined based on both weight (mol Mg g^{-1} s^{-1}, Fig. 2B) and mineral surface area (mol Mg m^{-2} s^{-1}, Fig. 2A). This is because previous authors have shown that there can be significant discrepancies between rates calculated using these two measurements (Qin and Beckingham, 2021) (see S.I. section S3 for details). For example, the forsterite reaction rate is faster than that of serpentine and hydrotalcite on a per surface area basis (Fig. 2A) but becomes the slowest on a per gram basis (Fig. 2B). Similarly, the dissolution rate of the synthetic pyroaurite increase by ~3 orders of magnitude when measuring rate per gram instead of normalizing to surface area (Fig. 2B) because the synthetic sample has a much higher BET surface area than the other minerals (66.1 m^2/g for the synthetic pyroaurite vs 4.15 m^2/g for the natural brucite). The main challenge associated with rate calculations using surface area is accurately capturing and characterizing the accessible reactive surface areas that account for surface roughness and variations in reactive site density of the mineral phase (White and Brantley, 2003; Azizi and Larachi, 2019). Additionally, Qin and Beckingham (2021) demonstrate orders of magnitude differences between various reactive surface area measuring techniques. This implies that reaction rates on a per gram basis are more suitable for polymineralic material such as tailings because it decouples it from the effect of reactive surface areas. Therefore, the rate comparison in Fig. 2B will be used for the rest of the discussion in this paper.

The tailings samples show a 2-stage dissolution pathway similar to those of the pure Mg-silicates, during which the Mg release rate in the transient stage is much faster than that at steady-state. In Fig. 2B, tailings with a higher abundance of brucite, such as BD1 (9 wt% brucite) and MKM (6 wt% brucite), react almost half an order of magnitude faster than BD2 (<3 wt% brucite, Fig. 2B). GK1, which has a brucite abundance below the detection limit (<0.3 wt% when using TGA), dissolved the slowest at a rate comparable to the pure serpentine sample. The reaction rate of BD1 plunged approximately two orders of magnitude upon releasing approximately 19% of the total Mg^{2+}, exhibiting a similar trend to the brucite sample when it approached 100% reaction. MKM released about 8% of the total Mg^{2+} before the rate dropped to below 10^{-9} mol Mg g^{-1} s^{-1}. In Fig. 2B, the serpentine dissolution rate shows a gradual decline while brucite shows a plateau followed by a sharp drop. Brucite-rich tailings mirror the dissolution behaviour of brucite, displaying a plateau with a sharp decline (i.e. BD1, MKM). Brucite-poor, serpentine-rich tailings demonstrate a gradual flattened rate, following the trend of serpentine dissolution (i.e.BD2, GK1). Based on these observations, the tailings dissolution rates can as expected be understood in the context of mineral content. Dissolution pathways of tailings are primarily constrained by brucite and serpentine abundance, with tailings containing more brucite dissolving faster (Fig. 2B).

When considering the need for carbon sequestration, not all mineral sources of divalent cations are equally useful. This is because the divalent cations need to dissolve and be released into solution on human time scales of months to years, rather than geological time scales, if they are reacted to form carbonates at a rate that could reduce climate change. Here, we describe the easily accessible cations as "labile" cations. For ultramafic rocks, minerals with a high abundance of Mg^{2+} are the most common divalent cation source, meaning that the primary labile cation in ultramafic mine wastes is Mg^{2+} (Power et al., 2009; Hamilton et al., 2018; Ruggieri and Gherardi, 2020; Bullock et al., 2021; Cutts et al., 2021). Hence, we use labile Mg^{2+} to quantify carbon sequestration reactivity in ultramafic rocks and define it as Mg^{2+} that is accessible and can be rapidly leached at ambient pressure and temperature for mineral carbonation. However, what can be considered as accessible will depend on the characteristics of a carbon sequestration site, particularly the length of time that the cation feedstock is exposed and can dissolve and react with CO_2 to form carbonates (e.g., duration of CO_2 injection or duration of tailings exposure to CO_2 in the atmosphere).

In Fig. 2B, we plot four 1:1 cutoff lines that show how rapidly a mineral or rock has to be releasing Mg into the solution to be considered labile Mg, given four different exposure or reaction times (1 day, 1 week, 1 month and 1 year). The starting point for each line is the dissolution rate required to dissolve 100% of the Mg^{2+} from a sample in the given time, which corresponds with dissolution rates of 1.67×10^{-7}, 2.3×10^{-8}, 5.4×10^{-9} and 4.5×10^{-10} mol Mg g^{-1} s^{-1}. Calculation of these rates follows the relationship of *dissolution rate* × *reaction time* = *amount*, assuming *amount* = 0.014 mol Mg^{2+} g^{-1} because this is the average total Mg^{2+} content of typical ultramafic minerals (i.e. brucite, serpentine, forsterite). They are 1:1 lines because it is assumed that if only a portion of a sample Mg^{2+} is accessible, then a lower reaction rate is required to dissolve all the easily accessible Mg in the given time frame. If a sample plot is entirely above a given cutoff line, it is wholly considered labile; if a sample plot is partially above and partially below a cutoff line, then the part above the cutoff line is the labile Mg^{2+} content. For example, using Fig. 2B, assuming a reaction time of one week (red cutoff line), we can see that almost all Mg^{2+} in the brucite sample is labile as it is almost entirely above the red line. However, the olivine and serpentine samples cross the red cutoff line at approximately 1% and 2% of their total Mg^{2+}, indicating that only these portions can be considered labile.

Tailings samples are assessed similarly. The high brucite nickel tailings sample (BD1) contains 19% labile Mg, while the kimberlite tailings with no brucite content (GK1) contains only 3.9% labile Mg. From Fig. 2B, we can see that portions of the Mg content for olivine and serpentine are labile, even when considering the shortest reaction time (1 day). Thus, labile Mg in ultramafic mine tailings comes from two sources A, bulk dissolution of highly reactive trace minerals (i.e. brucite and hydrotalcite); and B, the initial transient reaction of Mg-silicates (i.e. serpentine, olivine). Source A is important because even though Mg-hydroxides are present in trace abundances in ultramafic tailings, all their Mg^{2+} are labile. Source B is important because even though the labile Mg content is relatively low, the total abundance of the Mg-silicates can be very high. The labile content of Mg-silicates may represent the missing link that explains the faster than anticipated mineral carbonation rate documented at mine sites (Wilson et al., 2009, 2010, 2014), as many previous studies' predictions were based solely on the dissolution of trace phases and ignoring the initial transient dissolution of Mg-silicate minerals.

3.2. Labile Mg from serpentine vs olivine

Flow-through experimental results indicate that there are significant

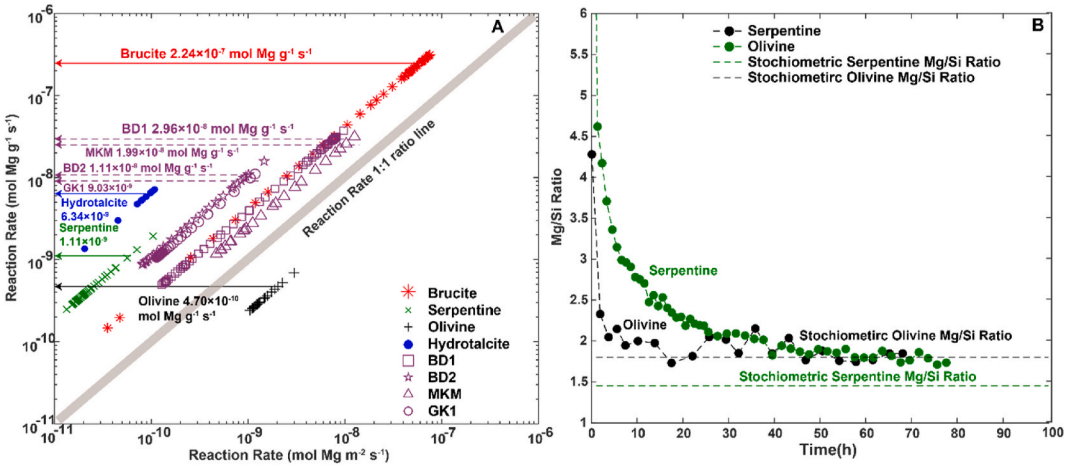

Fig. 3. (A) Comparison of reaction rate normalized with surface area (mol Mg m^{-2} s^{-1}) and mass (mol Mg g^{-1} s^{-1}); 1:1 indicates where rates are equal. The coloured arrow lines indicate the rate at the 3rd or the 4th measurement of the experiment. The labelled reaction rates are typically indicative of the plateau observed in Fig. 2. (B) Aqueous Mg/Si molar ratio versus time. The dashed black line indicates the olivine stochiometric Mg/Si ratio of 1.8; the dashed green line indicates the stochiometric Mg/Si ratio of serpentine 1.45.

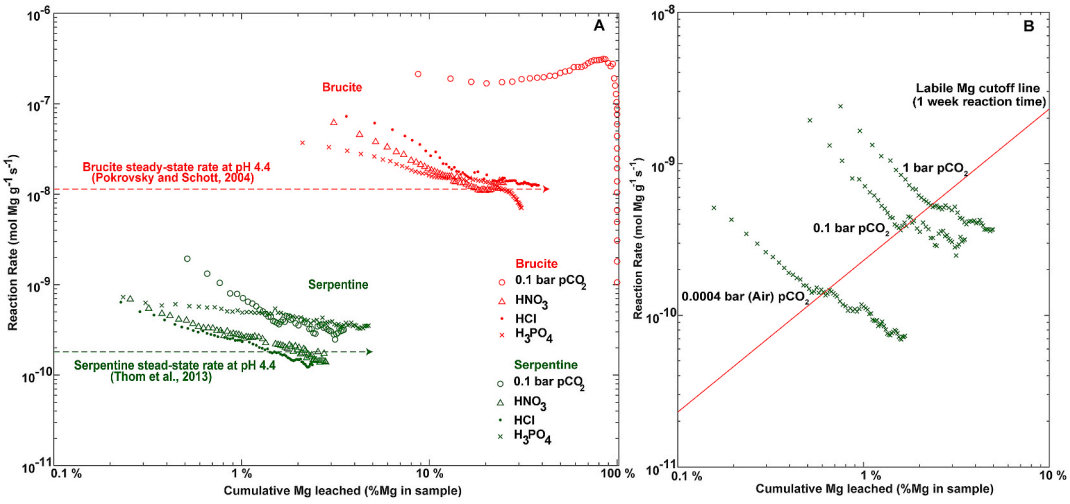

Fig. 4. (A) Brucite and serpentine dissolution rate (mol Mg g^{-1} s^{-1}) versus cumulative Mg leached (%) at pH 4.4 using HCl, HNO_3, H_3PO_4 and 0.1 bar pCO_2. The brucite and serpentine steady-state dissolution rates are indicated as red and green dashed lines. (B) Serpentine dissolution rate versus cumulative Mg leached in solution at 1 bar, 0.1 bar and 0.0004 bar pCO_2; the red 1:1 ratio line is the labile Mg cut-off at 1-week reaction time.

differences in the relative reactivity of olivine and serpentine which depend on how reaction rate is assessed. This observation contradicts earlier research that argued olivine always reacts faster and, therefore, has more significant geological carbon sequestration potential (O'Connor et al., 2002; Kelemen and Hirth, 2012; Li et al., 2018; Oelkers et al., 2018; Sun et al., 2019). Olivine (forsterite-Mg endmember: Mg_2SiO_4) is an unpolymerized orthosilicate that tends to dissolve more rapidly than phyllosilicates such as serpentine when normalized to the surface area of the material (Fig. 2A, Luce et al., 1972; Pokrovsky and Schott, 2004; De Baere et al., 2015). As serpentine has a relatively higher surface area and olivine has a relatively low surface area, this normalization favored the olivine dissolution rate. However, the experimental rate comparison results, normalized to sample mass, indicate that serpentine dissolution is five times faster than olivine (Fig. 2B). In Fig. 3, we further compared the two rate calculation methods and observed that dissolution rates of all samples are faster on a per mass basis than per area (higher than the 1:1 ratio line) except for olivine (Fig. 3). Given that dissolution for field-scale carbon sequestration is constrained by the mass of reactive material, normalizing the reaction rate to mass enables a more realistic comparison between minerals capacity for releasing labile Mg for use in carbon sequestration. These results agree with the previous conclusion that when considering materials for carbon sequestration, using a reaction rate normalized by mass is more suitable. Thus, the amount of labile Mg^{2+} sourced from olivine is much lower than that of serpentine because olivine dissolves slower.

In Fig. 3, the Mg:Si ratio of serpentine remained non-stoichiometric through to the end of the experiment. Olivine, on the other hand, reached steady-state dissolution after 15 h. These results suggest that there is correspondence between fast rate and non-stoichiometric dissolution. During the non-stoichiometric dissolution of Mg-silicates, rates tend to be faster than that at steady-state, and the transient period of serpentine dissolution is more extended than olivine. Serpentine dissolution experiments (Daval et al., 2013; Thom et al., 2013) have suggested that the rate of serpentine dissolution is initially highly non-stoichiometric due to the preferential release of Mg^{2+} from the surface 'brucite-like' sheets. In a pH-jump experiment presented in Thom et al. (2013), serpentine dissolution experiments showed steady-state dissolution increased significantly with a shift from pH 4 to 2. Thom et al. (2013) argued that the two dramatically different rates before and after the pH-jump indicated that the transience at the

beginning of serpentine dissolution is not a sample preparation artifact (i.e. dissolution of fine particles) but rather a response to the perturbation of the mineral surface (see section S2 in S.I. for details). In comparison, olivine has less accessible surface Mg^{2+} than serpentine because it has a smaller surface area (Olivine BET: 0.23 m^2/g, Serpentine BET: 18.5 m^2/g) and a shorter transient dissolution period (see S.I section S5 for details).

We posit that serpentine is a better candidate for mineral carbonation than olivine because 1) serpentine has a larger reactive surface area for labile Mg release from surface processes, and 2) serpentine dissolves at a non-stoichiometric rate faster and longer than olivine. These results contradict the commonly held belief that olivine is a better mineral candidate for carbon sequestration processes at earth surface conditions than serpentine.

3.3. Labile Mg dependence on acid types and pCO_2

Serpentine and brucite were subjected to dissolution in HCl, HNO_3 and H_2PO_4 to explore the effect of the reaction mechanism on cumulative Mg^{2+} leached (Fig. 4A). Serpentine was also dissolved in solution with various pCO_2 to test rate dependence on carbonic acid strength (Fig. 4B). In Fig. 4A, brucite and serpentine dissolution rates in HCl, HNO_3 are comparable with the steady-state rates determined in the literature (Vermilyea, 1969; Lin and Clemency, 1981; Jordan and Rammensee, 1996; Palandri and Kharaka, 2004; Pokrovsky and Schott, 2004; Harrison et al., 2013; Azizi and Larachi, 2019). Brucite steady-state dissolution rate at pH 4.4, adapted from Pokrovsky and Schott (2004) (1.14×10^{-8} mol Mg g^{-1} s^{-1}), is comparable with the rate of brucite dissolution in HCl and HNO_3. Brucite reaction rate in 0.1 bar pCO_2 solution ($\sim 10^{-7}$ mol Mg g^{-1} s^{-1}) is significantly higher than that for the other acid types ($\sim 10^{-8}$ mol Mg g^{-1} s^{-1}).

Results from serpentine dissolution results presented in Fig. 4 show acids that form inorganic ligands (i.e. HCO_3^-, $H_2PO_4^-$) promote the early-stage dissolution rates of serpentine and that serpentine dissolution rate increases linearly with pCO_2. Serpentine dissolution rates were enhanced in solutions with HCO_3^- and $H_2PO_4^-$, compared to solutions with only H^+. The steady-state dissolution of serpentine at pH 4.4 is 1.81×10^{-10} mol Mg g^{-1} s^{-1}. In Fig. 4A, the rate of serpentine dissolution in HCl and HNO_3 reached the steady-state rate after 4% of the total Mg^{2+} are leached. Transient dissolution prevailed during the serpentine dissolution and showed changes with aqueous composition and acidity. Incongruent serpentine dissolution is evident by the high Mg:Si molar ratio as shown in Fig. 4B, and that Mg is preferentially leached relative to Si throughout the experiment duration. The simultaneous drop in reaction rate and Mg:Si molar ratio indicates that serpentine dissolution is approaching stoichiometric dissolution near the end of the experiment. The total cumulative Mg^{2+} released from serpentine dissolution in H_3PO_4 is ~5% of the total Mg^{2+} compared to 4%, 2.75%, and 2.5% in 0.1 barCO_2, HCl, and HNO_3, respectively. Finally, the dissolution rate of serpentine during the incongruent stage also reveals strong pH dependence. In Fig. 4B, serpentine dissolves the fastest in solution with the highest pCO_2 and acidity (1 bar pCO_2, pH = 3.89). Cumulative Mg^{2+} obtained from the dissolution in the most acidic condition is around 5% of the total Mg^{2+}, compared to only 1% obtained from serpentine dissolution in solution with the lowest pCO_2 and acidity (0.0004 bar pCO_2, pH = 5.60).

Inorganic ligands, such as sulphate, carbonate and phosphate, can enhance mineral dissolution rates by forming surface complexes (Pokrovsky et al., 2005). The effect of carbonate ligands on mineral dissolution rates is of particular relevance for mineral carbonation. Pokrovsky et al. (2005) demonstrated that acids that form protonated ions (e.g., HCO_3^- and $H_2PO_4^-$) at neutral to weakly alkaline pH conditions promote dissolution, whereas those that form deprotonated ions (e.g., CO_3^{2-} and PO_4^{3-}) may inhibit dissolution. Harrison et al. (2013) also showed that brucite dissolution is a surface-controlled reaction that can be accelerated via the direct effect of increasing HCO_3^- concentration and the indirect effect of increasing acidity. Brucite is completely consumed while reacting in solution with CO_2, indicated by the rapid decline in reaction rate after reaching 100% cumulative Mg^{2+} leached. XRD analysis of solid after the experiment showed that brucite completely disappeared after reaction in solution with CO_2. The total sample mass loss, calculated from the cumulative [Mg^{2+}] in the effluent, also corresponds to the proportion of brucite in the unreacted sample. These findings suggest that the mechanisms for enhancing dissolution kinetics vary by acid type. Acids that form protonated ions, which form ligands, will promote dissolution via ligands, while acids that don't form protonated ions (e.g., HCl and HNO_3) will promote dissolution via increasing acidity.

Table 3
Correction factor (a, b, c) values for calculating labile Mg content at various pCO_2.

Correction Factors	0.0004 bar pCO_2	0.1 bar pCO_2	1 bar pCO_2
a (Brucite)	1[a]	1[a]	1[a]
b (Serpentine)	0.0062	0.02	0.025
c (Olivine)	<0.01[a]	<0.01[a]	0.01[a]

[a] Values of a and c are constant because brucite and olivine are the fastest and slowest dissolving minerals.

The flow-through dissolution results indicate that protons and inorganic ligands can promote serpentine dissolution the same way as it does for brucite. Like brucite, the early-stage serpentine dissolution rate is a surface process that can be accelerated via hydration of CO_2 in mildly acidic conditions. The effect of inorganic HCO_3^- and $H_2PO_4^-$ ligands on the serpentine surface follows a surface complexation and coordination framework. Ligands adsorbed on the serpentine surface attack the Mg–O bonds, facilitating the Mg^{2+} detachment from the surface (Pokrovsky et al., 2005). The exchange rate of water molecules around Mg^{2+} centers is thus faster, allowing the rapid dissolution of Mg^{2+} at the mineral surface. Until now, ligand-promoted activation has been an overlooked dissolution pathway for the incongruent transient stage of serpentine dissolution. Our experimental results demonstrate that serpentine dissolution kinetics and extractable Mg^{2+} change with both dissolution mechanism and pCO_2. For one week residence time, serpentine labile Mg content at 1 bar pCO_2 (pH = 3.89) is the highest (~3% of total Mg^{2+}) compared to that at 0.0004 bar pCO_2 (pH = 5.6) (0.62% of total Mg^{2+}), suggesting a positive correlation between labile Mg, pH and CO_2 concentration (Fig. 4B). It is fortunate that brucite and serpentine labile Mg content increase with acid strength and the presence of ligands like CO_2, given that the most likely acid source at an ultramafic mine site would be carbonic acid derived from CO_2 rich gas streams.

3.4. Calculating labile Mg from mineralogy

Tailings characterization data can be used with flow-through leach tests to predict mineral carbonation reactivity. For this purpose, the mineral dissolution behaviours are categorized into two classes. Class-one minerals are fast-reacting with no distinction of congruent or incongruent dissolution (e.g. brucite, hydrotalcite group minerals). All Mg^{2+} found in class-one minerals are labile. Minerals with fast, incongruent dissolution at the surface are categorized as class two. The labile Mg content in these minerals is minimal compared to their total Mg^{2+} but can still be significant if they constitute a primary mineral of the feedstock. Serpentine and olivine are class-two minerals where 1–6% of their total Mg^{2+} can be labile depending on the chemical conditions and reaction time. Using mineral characterization data from qXRD and TGA, the labile Mg content of the tailings samples was estimated using Eq (3).

$$Labile\ Mg(wt\%) = a\left(B_{wt\%} \cdot B_{Mg\ wt\%}\right) + b\left(S_{wt\%} \cdot S_{Mg\ wt\%}\right) + c\left(O_{wt\%} \cdot O_{Mg\ wt\%}\right) \quad (3)$$

where $B_{wt\%}$ is the brucite abundance measured using TGA; $S_{wt\%}$ and $O_{wt\%}$ are wt% of serpentine and olivine (forsterite) based on XRD mineral

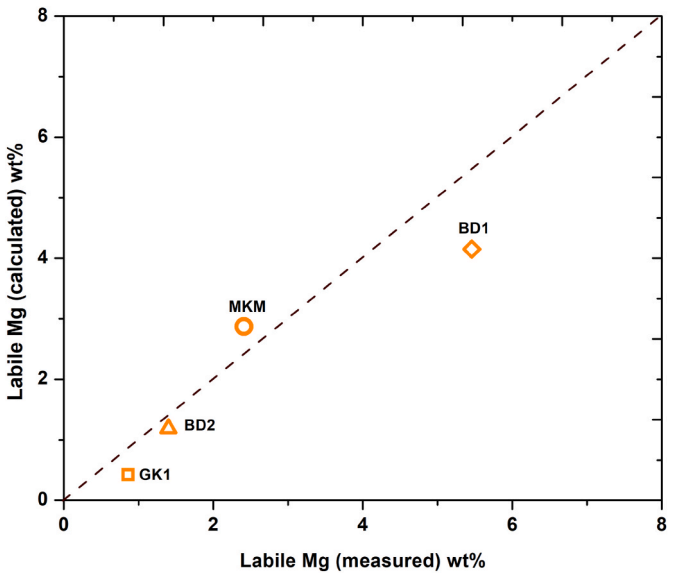

Fig. 5. Calculated versus measured labile Mg % of total Mg in tailings samples.

abundance; $B_{Mg\%}$, $S_{Mg\%}$ and $O_{Mg\%}$ are the total Mg content in brucite, serpentine and olivine; and a, b, c are factors that correct for labile Mg content in brucite, serpentine and olivine. These factors are different at various CO_2 concentrations (Table 3). Typical MgO contents in brucite, serpentine and olivine are 41.68%, 26.31% and 34.55%, respectively. However, these values are not built into the equation because Mg content in these minerals can vary by deposit and rock types (Frost 2003; Andreani et al., 2008). For example, the substitution of Fe for Mg in brucite can range from 6 to 72 mol %, meaning that Mg% of minerals from different localities can change the accuracy of labile Mg calculation (Hostetler et al., 1966). At 0.1 bar pCO_2 and one week reaction time, we counted 100%, 2% and 1% of the total Mg^{2+} in brucite, serpentine and olivine as labile and calculated labile Mg content of the four tailings samples. The results are compared with measurements from the flow-through experiments and are shown in Fig. 5. Of the four tailings samples, BD1 and MKM are nickel tailings with high to intermediate brucite and serpentine abundance. Their estimated labile Mg content can be a bit different compared to that measured in experiments (BD1: 4.15 versus 5.46; MKM: 2.87 versus 2.4). Overall, labile Mg content calculated is comparable with our measured results using flow-through. This means, with sufficient mineralogical information, the mineral carbonation reactivity can be estimated using labile Mg content. Among the empirical constraints determined for labile Mg, tailings mineral abundance is the most significant factor for characterizing mineral carbonation reactivity. The effect of geochemical conditions such as pCO_2 and reaction time can further refine labile Mg estimation and provide more accurate reactivity assessments. Furthermore, the concept of labile cations for accessing carbon sequestration potential is applicable to other industrial wastes that may be a sink for atmospheric CO_2. For example, labile Ca can be estimated, for typical mafic materials, such as plagioclase and natural volcanic glasses.

3.5. Implications for carbon sequestration

To evaluate whether the CO_2 sequestration capacity of mine tailings can provide a pathway for significantly reducing the greenhouse gas footprint of mine operations, we estimated the carbon capture potential of the four tailings samples and compared them to the mine emissions for each site (Fig. 6). In Fig. 6, labile Mg is converted to carbon capture potential in tonnes CO_2 per tonne of tailings to compare with mine emissions. The coloured bars represent the labile Mg content of the GK1, BD2, MKM and BD1 tailings samples. They are ranked by brucite content from ~0.1 wt% to ~10 wt% to represent a range of tailings mineralogy. Serpentine labile Mg in 100%CO_2, 10%CO_2 and air CO_2 contributes to the variation of these computed labile Mg numbers. As shown in Fig. 6, the carbon offset provided by tailings with the second-lowest brucite content (1.7 wt%) would be sufficient to make mine sites such as the

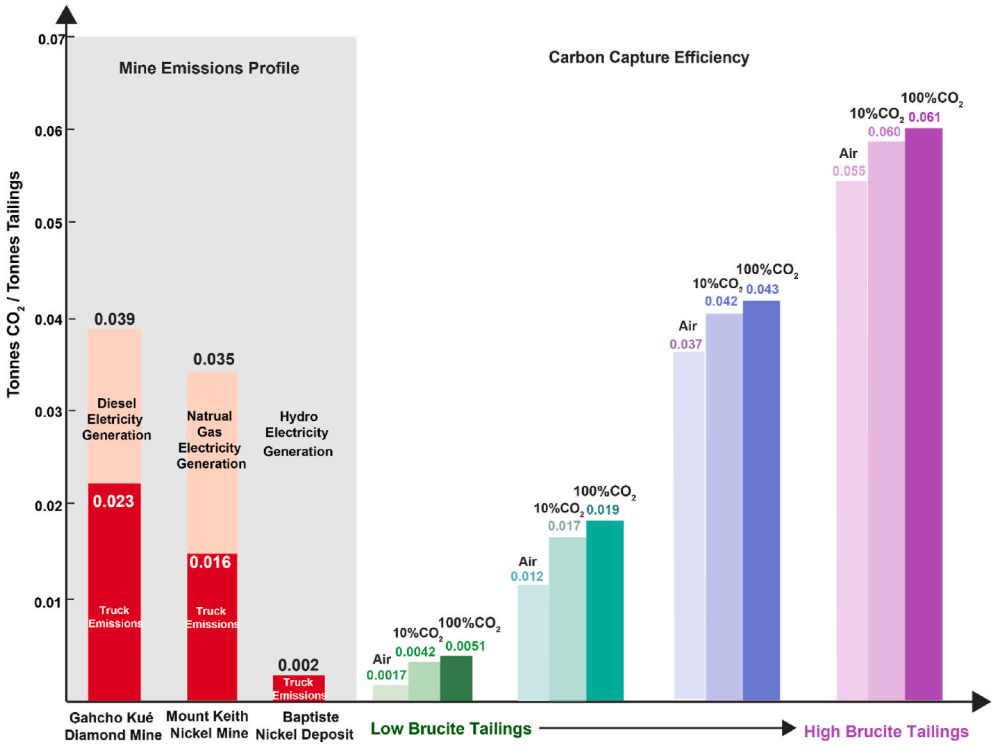

Fig. 6. Mine emissions profile of the Mount Keith nickel mine (Wilson et al., 2014), Gahcho Kué diamond mine (De Beers Group, 2019), and Baptiste nickel deposit (FPX Nickel, 2022) compared with the carbon capture efficiency of tailings with various brucite contents (0.1, 1.7, 5.9 and 8.9 wt%) and CO_2 concentration.

Baptiste Nickel deposit carbon negative and could offset carbon emissions from electricity generation at a mine site like Mount Keith. For mines like Gahcho Kué where the diesel consumption splits between electricity generation and truck emissions, flue gas from using diesel for electricity generation on-site represents a significant opportunity to access a stream of concentrated CO_2. The relatively small difference in labile Mg content when using 10%CO_2 versus 100%CO_2 means that moderately concentrated CO_2 sources such as flue gas can achieve a similar carbonation rate as purified CO_2, which is highly advantageous as it eliminates the cost of purifying CO_2. Overall, labile cation availability and quantity can directly affect the ability of a mine to sequester carbon.

4. Conclusions

In this study, flow-through dissolution experimental results have demonstrated that mineral samples and mine tailings have two stages of dissolution: fast releasing labile cations that have value for the short-term implementation of mineral carbonation and a long-term bulk cation release that is challenging to use in carbon capture and storage technologies. The labile cations are sourced from trace minerals with a high reaction rate and non-stoichiometric surface reaction processes that are missing from most geochemical models for mineral weathering. Labile cations represent mine tailings reactivity for carbon capture and storage and are controlled by the pre-existing mineral composition and geochemical conditions. Reaction time and transient rate are the key factors that determine labile cations' amount. The change from initial rapid dissolution to slower long-term dissolution has implications for experiments that attempt to demonstrate rapid carbon sequestration rate in scenarios like subsurface injection (Oelkers et al., 2018; Clark et al., 2020) and soil amendment (Washbourne et al., 2012; Beerling et al., 2018, 2020). If the initial storage success comes from the early stage of dissolution, it is possible it may not be representative of long-term reactivity and extrapolating those results to the long-term may result in a significant overestimation of carbon capture potential. An improved understanding of mineral reactivity in the short and long term is key to accurately assessing carbon sequestration capacity.

Author contributions

The manuscript was written through the contributions of all authors. All authors have given approval to the final version of the manuscript.

Declaration of competing interest

The authors declare the following financial interests/personal relationships which may be considered as potential competing interests: Gregory M. Dipple reports financial support was provided by Natural Sciences and Engineering Research Council of Canada.

Acknowledgment

We acknowledge the grant support of the Natural Sciences and Engineering Research Council of Canada (NSERC) Discovery Grant to GMD. Additional support (International Tuition Award, Special UBC Graduate Scholarship, W.H. MATHEWS Scholarship, Colin D Spence Memorial Scholarship in Geology and Thomas and Marguerite MacKay Memorial Scholarship) provided by the University of British Columbia, Department of Earth, Ocean and Atmosphere Science. We thank Maureen Soon for her experimental and analytical assistance. We appreciate Dr. Uli Mayer's advice regarding geochemical modelling and Dr. Bart De Baere and Dr. Roger Francois for adopting the in-line flow-through time-resolved analysis (FT-TRA) module for experiments.

Appendix A. Supplementary data

Supplementary data to this article can be found online at https://doi.org/10.1016/j.apgeochem.2022.105285.

References

Amram, K., Ganor, J., 2005. The combined effect of pH and temperature on smectite dissolution rate under acidic conditions. Geochem. Cosmochim. Acta 69 (10), 2535–2546. https://doi.org/10.1016/j.gca.2004.10.001.

Andreani, M., Grauby, Olivier, Baronnet, Alain, Munoz, Manuel, 2008. Occurrence, composition and growth of polyhedral serpentine. Eur. J. Mineral 20, 159–171. https://doi.org/10.1127/0935-1221/2008/0020-1801.

Aoba, T., Shimoda, S., Moreno, E.C., 1992. Labile or surface pools of magnesium, sodium, and potassium in developing porcine enamel mineral. J. Dent. Res. 71 (11), 1826–1831. https://doi.org/10.1177/00220345920710111201.

Arce, Gretta L.A.F., Soares Neto, T.G., Avila, I., Luna, C.M.R., Carvalho, J.A., 2017. Leaching optimization of mining wastes with lizardite and brucite contents for use in indirect mineral carbonation through the pH swing method. J. Clean. Prod. 141, 1324–1336.

Assima, G.P., Larachi, F., Beaudoin, G., Molson, J., 2012. CO2 sequestration in chrysotile mining residues-implication of watering and passivation under environmental conditions. Industrial and Engineering Chemistry Research 51 (26), 8726–8734. https://doi.org/10.1021/ie202693q.

Azizi, D, Larachi, F, 2019 Jan. Surface Speciation of Brucite Dissolution in Aqueous Mineral Carbonation: Insights from Density-Functional Theory Simulations. J. Phys. Chem. A. 123 (4), 889–905. https://doi.org/10.1021/acs.jpca.8b09140. PMID: 30633523.

Béarat, H., Mckelvy, M.J., Chizmeshya, A., Gormley, D., Nunez, R., Carpenter, R., Squires, K., Wolf, G., 2006. Carbon sequestration via aqueous olivine mineral carbonation: role of passivating layer formation. Environ. Sci. Technol. 40 (15), 4802–4808. https://doi.org/10.1021/es0523340.

Beaudoin, G., Nowamooz, A., Assima, G.P., Lechat, K., Gras, A., Entezari, A., Fortier, R., 2017. Passive mineral carbonation of Mg-rich mine wastes by atmospheric CO2. Energy Proc. 114, 6083–6086. https://doi.org/10.1016/j.egypro.2017.03.1745. November 2016.

Beerling, D.J., Kantzas, E.P., Lomas, M.R., et al., 2020. Potential for large-scale CO_2 removal via enhanced rock weathering with croplands. Nature 583, 242–248. https://doi.org/10.1038/s41586-020-2448-9.

Beerling, D.J., Leake, J.R., Long, S.P., Scholes, J.D., Ton, J., Nelson, P.N., Hansen, J., 2018. Farming with crops and rocks to address global climate, food and soil security. Nature Plants 4 (3), 138–147. https://doi.org/10.1038/s41477-018-0108-y.

Bondietti, G., Sinniger, J., Stumm, W., 1993. The reactivity of F.E. (III) (hydr)oxides: effects of ligands in inhibiting the dissolution. Colloids Surf. A Physicochem. Eng. Asp. 79 (2–3), 157–167. https://doi.org/10.1016/0927-7757(93)80171-A.

Bullock, L.A., James, R.H., Matter, J., Renforth, P., Teagle, D.A.H., 2021. Global carbon dioxide removal potential of waste materials from metal and diamond mining. Frontiers in Climate 3 (July). https://doi.org/10.3389/fclim.2021.694175.

Cama, J., Ganor, J., 2006. The effects of organic acids on the dissolution of silicate minerals: a case study of oxalate catalysis of kaolinite dissolution. Geochem. Cosmochim. Acta 70 (9), 2191–2209. https://doi.org/10.1016/j.gca.2006.01.028.

Clark, Deirdre, Oelkers, Eric, Gunnarsson, Ingvi, Sigfusson, Bergur, Snæbjörnsdóttir, Sandra Ó., Aradottir, Edda, Gislason, Sigurdur, 2020. CarbFix2: CO2 and H2S mineralization during 3.5 years of continuous injection into basaltic rocks at more than 250 °C. Geochem. Cosmochim. Acta 279, 45–66. https://doi.org/10.1016/j.gca.2020.03.039.

Cutts, J.A., Steinthorsdottir, K., Turvey, C., Dipple, G.M., Enkin, R.J., Peacock, S.M., 2019. Deducing mineralogy of serpentinized and carbonated ultramafic rocks using physical properties with implications for carbon sequestration and subduction zone dynamics. G-cubed 22 e2021GC009989. https://doi.org/10.1029/2021GC009989.

Daval, D., Hellmann, R., Martinez, I., Gangloff, S., Guyot, F., 2013. Lizardite serpentine dissolution kinetics as a function of pH and temperature, including effects of elevated pCO2. Chem. Geol. 351, 245–256. https://doi.org/10.1016/j.chemgeo.2013.05.020.

De Baere, B., François, R., Mayer, K.U., 2015. Measuring mineral dissolution kinetics using on-line flow-through time-resolved analysis (FT-TRA): an exploratory study with forsterite. Chem. Geol. 413, 107–118. https://doi.org/10.1016/j.chemgeo.2015.08.024.

De Beers Group, 2019. Gahcho Kué Mine 2019 Annual Air Quality Report, pp. 1–48. August.

Eloneva, S., Teir, S., Salminen, J., Fogelholm, C.J., Zevenhoven, R., 2008. Fixation of CO2 by carbonating calcium derived from blast furnace slag. Energy 33 (9), 1461–1467. https://doi.org/10.1016/j.energy.2008.05.003.

Fagerlund, J., Nduagu, E., Romão, I., Zevenhoven, R., 2012. CO2 fixation using magnesium silicate minerals part 1: process description and performance. Energy 41 (1), 184–191. https://doi.org/10.1016/j.energy.2011.08.032.

FPX Nickel, 2022. *FPX Nickel Reports Expanded Field Tests Demonstrating the Baptiste Deposit has Unique Potential to Become the Nickel Industry's First Large-Scale, Carbon-Neutral Operation - FPX Nickel.* [online] Available at: <https://fpxnickel.com/2021/06/fpx-nickel-reports-expanded-field-tests-demonstrating-the-baptiste-deposit-has-unique-potential-to-become-the-nickel-industrys-first-large-scale-carbon-neutral-operation/> [Accessed 26 March 2021].

Frost, Daniel, 2003. Fe2+ - Mg partitioning between garnet, magnesiowüstite, and (Mg, Fe)2SiO4 phases of the transition zone. Am. Mineral. 88, 387–397. https://doi.org/10.2138/am-2003-2-315.

Gerdemann, S.J., O'Connor, W.K., Dahlin, D.C., Penner, L.R., Rush, H., 2007. Ex situ aqueous mineral carbonation. Environ. Sci. Technol. 41 (7), 2587–2593. https://doi.org/10.1021/es0619253.

Gislason, Sigurdur, Broecker, W.S., Gunnlaugsson, E., Snæbjörnsdóttir, Sandra Ó., Mesfin, Kiflom, Alfredsson, Helgi, Aradottir, Edda, Sigfusson, Bergur, Gunnarsson, I., Stute, Martin, Matter, Juerg, Arnarson, M.Th, Galeczka, Iwona, Gudbrandsson, S., Stockmann, Gabrielle, Wolff-Boenisch, Domenik, Stefansson, Andri, Ragnheidardottir, E., Flaathen Loe, K., Therese, Oelkers, Eric, 2014. Rapid solubility and mineral storage of CO2 in basalt. Energy Proc. 63, 4561–4574. https://doi.org/10.1016/j.egypro.2014.11.489.

Hamilton, J.L., Wilson, S.A., Morgan, B., Turvey, C.C., Paterson, D.J., Jowitt, S.M., McCutcheon, J., Southam, G., 2018. Fate of transition metals during passive carbonation of ultramafic mine tailings via air capture with potential for metal resource recovery. Int. J. Greenh. Gas Control 71, 155–167.

Han, Sang-Jun, Im, Hye, Wee, Jung-Ho, 2015. Leaching and indirect mineral carbonation performance of coal fly ash-water solution system. Appl. Energy 142, 247–282. https://doi.org/10.1016/j.apenergy.2014.12.074.

Harrison, A.L., Power, I.M., Dipple, G.M., 2013. Accelerated carbonation of brucite in mine tailings for carbon sequestration. Environ. Sci. Technol. 47 (1), 126–134. https://doi.org/10.1021/es3012854.

Hellevang, Helge, 2015. Carbon capture and storage (CCS). In: Petroleum Geoscience: From Sedimentary Environments to Rock Physics, Second Edition, pp. 591–602. https://doi.org/10.1007/978-3-642-34132-8_24.

Hills, Colin, Tripathi, Nimisha, Carey, Paula, 2020. Mineralization technology for carbon capture, utilization, and storage. Front. Energy Res. 8, 142. https://doi.org/10.3389/fenrg.2020.00142.IPCC (2018). Global Warming of 1.5°C. Global Warming of 1.5°C. An IPCC Special Report on the Impacts of Global Warming of 1.5°C above Pre-Industrial Levels and Related Global Greenhouse Gas Emission Pathways, in the Context of Strengthening the Global Response to the Threat of Climate Change.

Hostetler, P.B., Coleman, R.G., Mumpton, F.A., Evans, B.W., 1966. Brucite in alpine serpentinites. Am. Mineral. 51 (1–2), 75–98.

IPCC. (2018). Global Warming of 1.5°C. An IPCC Special Report on the Impacts of Global Warming of 1.5°C above Pre-Industrial Levels and Related Global Greenhouse Gas Emission Pathways, in the Context of Strengthening the Global Response to the Threat of Climate Change,.

IPCC, 2021. IPCC press release AR6. Clim. Change 2013 - Phys. Sci. Basis 1–6. August 2021.

Jordan, G., Rammensee, W., 1996. Dissolution rates and activation energy for dissolution of brucite (001): a new method based on the microtopography of crystal surfaces. Geochem. Cosmochim. Acta 60 (24), 5055–5062. https://doi.org/10.1016/S0016-7037(96)00309-2.

Kandji, E.H.B., Plante, B., Bussière, B., Beaudoin, G., Dupont, P.P., 2017a. Geochemical behavior of ultramafic waste rocks with carbon sequestration potential: a case study of the Dumont Nickel Project, Amos, Québec. Environ. Sci. Pollut. Control Ser. 24 (12), 11734–11751. https://doi.org/10.1007/s11356-017-8735-9.

Kandji, E.H.B., Plante, B., Bussière, B., Beaudoin, G., Dupont, P.P., 2017b. Kinetic testing to evaluate the mineral carbonation and metal leaching potential of ultramafic tailings: case study of the Dumont Nickel Project, Amos, Québec. Appl. Geochem. 84, 262–276. https://doi.org/10.1016/j.apgeochem.2017.07.005.

Kelemen, P.B., Hirth, G., 2012. Reaction-driven cracking during retrograde metamorphism: olivine hydration and carbonation. Earth Planet Sci. Lett. 345-348, 81–89. https://doi.org/10.1016/j.epsl.2012.06.018.

Kelemen, P.B., Matter, J., 2008. In Situ Carbonation of Peridotite for CO2 Storage. Proceedings of the National Academy of Sciences of the United States of America. https://doi.org/10.1073/pnas.0805794105.

Koukouzas, N., Ziogou, F., Gemeni, V., 2009. Preliminary assessment of CO2 geological storage opportunities in Greece. Int. J. Greenh. Gas Control 3 (4), 502–513. https://doi.org/10.1016/j.ijggc.2008.10.005.

Krevor, S.C.M., Lackner, K.S., 2011. Enhancing serpentine dissolution kinetics for mineral carbon dioxide sequestration. Int. J. Greenh. Gas Control 5 (4), 1073–1080. https://doi.org/10.1016/j.ijggc.2011.01.006.

Lechat, Karl, Lemieux, Jean-Michel, Molson, John, Beaudoin, Georges, Hébert, Réjean, 2016. Field evidence of CO2 sequestration by mineral carbonation in ultramafic milling wastes, Thetford Mines, Canada. Int. J. Greenh. Gas Control 47, 110–121. https://doi.org/10.1016/j.ijggc.2016.01.036.

Li, J., Hitch, M., Power, I., Pan, Y., 2018. Integrated mineral carbonation of ultramafic mine deposits—a review. Minerals 8 (4), 147. https://doi.org/10.3390/min8040147.

Lin, F.C., Clemency, C.V., 1981. The dissolution kinetics of brucite, antigorite, talc, and phlogopite at room temperature and pressure. Am. Mineral. 66 (7–8), 801–806.

Liu, Qiang, Liu, Weizao, Hu, Jinpeng, Wang, Lin, Gao, Jianqiu, Liang, Bin, Yue, Hairong, Guoquan, Zhang, Luo, Dongmei, Li, Chun, 2018. Energy-efficient mineral carbonation of blast furnace slag with high value-added products. J. Clean. Prod. 197 https://doi.org/10.1016/j.jclepro.2018.06.150.

Luce, R.W., Bartlett, R.W., Parks, G.A., 1972. Dissolution kinetics of magnesium silicates. Geochem. Cosmochim. Acta 36 (1), 35–50. https://doi.org/10.1016/0016-7037(72)90119-6.

Matter, J.M., Broecker, W.S., Stute, M., Gislason, S.R., Oelkers, E.H., Stefánsson, A., Björnsson, G., 2009. Permanent carbon dioxide storage into basalt: the CarbFix pilot project, Iceland. Energy Proc. 1 (1), 3641–3646. https://doi.org/10.1016/j.egypro.2009.02.160.

McGrail, B., Schaef, Todd, Spane, Frank, Cliff, John, Qafoku, Odeta, Horner, Jake, Thompson, Christopher, Owen, Antoinette, Sullivan, Charlotte, 2016. Field validation of supercritical CO 2 reactivity with basalts. Environ. Sci. Technol. Lett. 4 https://doi.org/10.1021/acs.estlett.6b00387.

Melchiorre, E.B., Bottrill, R., Huss, G.R., Lopez, A., 2017. Conditions of stichtite (Mg6Cr2(OH)16[CO3]·4H2O) formation and its geochemical and isotope record of early phanerozoic serpentinizing environments. Geochimica et Cosmochimica Acta. https://doi.org/10.1016/j.gca.2016.10.020.

Mellini, M., 1982. The crystal structure of lizardite 1T: hydrogen bonds and polytypism. Am. Mineral. 67 (5–6), 587–598.

Metz, Volker, Ganor, Jiwchar, 2001. Stirring effect on kaolinite dissolution rate. Geochimica Et Cosmochimica Acta 65, 3475–3490. https://doi.org/10.1016/S0016-7037(01)00686-X.

Miller, V.S., Naeth, M.A., 2017. Amendments and substrates to develop anthroposols for northern mine reclamation. Can. J. Soil Sci. 97 (2), 266–277. https://doi.org/10.1139/cjss-2016-0145.

Mills, S.J., Christy, A.G., Génin, J.-M.R., Kameda, T., Colombo, F., 2012. Nomenclature of the hydrotalcite supergroup: natural layered double hydroxides. Mineral. Mag. 76 (5), 1289–1336. https://doi.org/10.1180/minmag.2012.076.5.10.

Murphy, W.M., Helgeson, H.C., 1987. Thermodynamic and kinetic constraints on reaction rates among minerals and aqueous solutions. III. Activated complexes and the pH-dependence of the rates of feldspar, pyroxene, wollastonite, and olivine hydrolysis. Geochem. Cosmochim. Acta 51 (12), 3137–3153. https://doi.org/10.1016/0016-7037(87)90124-4.

Oelkers, E.H., Gislason, S.R., Matter, J., 2008. Mineral carbonation of CO2. Elements 4 (5), 333–337. https://doi.org/10.2113/gselements.4.5.333.

Oelkers, E.H., Declercq, J., Saldi, G.D., Gislason, S.R., Schott, J., 2018. Olivine dissolution rates : a critical review 500 (June), 1–19. https://doi.org/10.1016/j.chemgeo.2018.10.008.

O'Connor, W.K., Dahlin, D.C., Rush, G.E., et al., 2002. Carbon dioxide sequestration by direct mineral carbonation: process mineralogy of feed and products. Min. Metallur. & Explor. 19, 95–101. https://doi.org/10.1007/BF03403262.

Palandri, J.L., Kharaka, Y.K., 2004. A Compilation of Rate Parameters of Water-Mineral Interctions Kinetics for Application to Geochemical Modeling. USGS-Report (2004-1068), Menlo Park, California, USA.

Parkhurst D.L., Appelo C.A.J. (2013) Description of input and examples for PHREEQC version 3—a computer program for speciation, batch-reaction, one-dimensional transport, and inverse geochemical calculations. US Geological Survey Techniques and Methods, book 6, chap A43, p 497.

Paulo, Carlos, Power, Ian, Stubbs, Amanda, Wang, Baolin, Zeyen, Nina, Wilson, Siobhan, 2021. Evaluating feedstocks for carbon dioxide removal by enhanced rock weathering and CO2 mineralization. Appl. Geochem. 129, 104955. https://doi.org/10.1016/j.apgeochem.2021.104955.

Pokrovsky, Oleg S., Schott, J., 2000. Kinetics and mechanism of forsterite dissolution at 25 ° C and pH from 1 to 12. Geochem. Cosmochim. Acta 64 (19), 3313–3325.

Pokrovsky, Oleg S., Schott, J., 2004. Experimental study of brucite dissolution and precipitation in aqueous solutions: surface speciation and chemical affinity control. Geochem. Cosmochim. Acta 68 (1), 31–45. https://doi.org/10.1016/S0016-7037(03)00238-2.

Pokrovsky, Oleg S., Schott, J., Castillo, A., 2005. Kinetics of brucite dissolution at 25°C in the presence of organic and inorganic ligands and divalent metals. Geochem. Cosmochim. Acta 69 (4), 905–918. https://doi.org/10.1016/j.gca.2004.08.011.

Power, Ian, Wilson, Siobhan, Thom, James, Dipple, Greg, Gabites, Janet, Southam, Gordon, 2009. The hydromagnesite playas of Atlin, British Columbia, Canada: a biogeochemical model for CO2 sequestration. Chem. Geol. 286–300. https://doi.org/10.1016/j.chemgeo.2009.01.012.

Power, Ian, Harrison, Anna, Dipple, Greg, Wilson, Siobhan, Kelemen, Peter, Hitch, Michael, Southam, Gordon, 2013. Carbon mineralization: from natural analogues to engineered systems. Rev. Mineral. Geochem. 77, 305–360. https://doi.org/10.2138/rmg.2013.77.9.

Pronost, J., Beaudoin, G., Tremblay, J., Larachi, F., Duchesne, J., Hébert, R., Constantin, M., 2011. Carbon sequestration kinetic and storage capacity of ultramafic mining waste. Environ. Sci. Technol. 45 (21), 9413–9420. https://doi.org/10.1021/es203063a.

Qin, F., Beckingham, L.E., 2021. The impact of mineral reactive surface area variation on simulated mineral reactions and reaction rates. Appl. Geochem. 124 https://doi.org/10.1016/j.apgeochem.2020.104852. December 2020.

Ragnheidardottir, E., Sigurdardottir, H., Kristjansdottir, H., Harvey, W., 2011. Opportunities and challenges for CarbFix: an evaluation of capacities and costs for the pilot scale mineralization sequestration project at Hellisheidi, Iceland and beyond. Int. J. Greenh. Gas Control 5 (4), 1065–1072. https://doi.org/10.1016/j.ijggc.2010.11.010.

Raudsepp, M., Pani, E., Dipple, G.M., 1999. Measuring mineral abundance in skarn; I, The Rietveld method using X-ray powder-diffraction data. Can. Mineral. 37 (1), 1–15.

Razote, Bernard, Jomari, Maranan, Mark, Eusebio, Ramon, Alorro, Richard, Beltran, Arnel, Orbecido, Aileen, 2019. Determination of the carbon dioxide sequestration potential of a nickel mine mixed dump through leaching tests. Energies 12, 2877. https://doi.org/10.3390/en12152877.

Ruggieri, G., Gherardi, F., 2020. In: Ruggieri, Giovanni, Gherardi, Fabrizio (Eds.), Geological and mineralogical sequestration of CO_2. Minerals, p. 198. ISBN 978-3-03936-876-1 (Hbk). https://doi.org/10.3390/books978-3-03936-877-8.

Sanna, A., Uibu, M., Caramanna, G., Kuusik, R., Maroto-Valer, M.M., 2014. A review of mineral carbonation technologies to sequester CO2. Chem. Soc. Rev. 43 (23), 8049–8080. https://doi.org/10.1039/c4cs00035h.

Seifritz, W., 1990. CO2 disposal by means of silicates [12]. Nature 345, 486. https://doi.org/10.1038/345486b0.

Seyama, H., Soma, M., Tanaka, A., 1996. Surface characterization of acid-leached olivines by X-ray photoelectron spectroscopy. Chem. Geol. 129 (3–4), 209–216. https://doi.org/10.1016/0009-2541(95)00142-5.

Sipilä, J., Teir, S., Zevenhoven, R., 2008. Carbon Dioxide Sequestration by Mineral Carbonation Literature Review Update 2005–2007. Akademi University Faculty of Technology Heat Engineering Laboratory. https://doi.org/10.1080/00908310600628263.

Snæbjörnsdóttir, S., Gislason, S.R., Galeczka, I.M., Oelkers, E.H., 2018. Reaction path modelling of in-situ mineralisation of CO2 at the CarbFix site at Hellisheidi, SW-Iceland. Geochem. Cosmochim. Acta 220, 348–366. https://doi.org/10.1016/j.gca.2017.09.053.

Songolzadeh, M., Soleimani, M., Takht Ravanchi, M., Songolzadeh, R., 2014. Carbon dioxide separation from flue gases: a technological review emphasizing reduction in greenhouse gas emissions. TheScientificWorldJournal, 828131. https://doi.org/10.1155/2014/828131.

Stumm, W., 1997. Reactivity at the mineral-water interface: dissolution and inhibition. Colloids Surf. A Physicochem. Eng. Asp. 120 (1–3), 143–166. https://doi.org/10.1016/S0927-7757(96)03866-6.

Stumm, W., Wehrli, Bernhard, Wieland, Erich, 1987. Surface complexation and its impact on geochemical kinetics. Croatica Chemica Acta 60, 429–456.

Sun, J. zhi, Wen, J., kang, Chen, wei, B., Wu, B., 2019. Mechanism of Mg^{2+} dissolution from olivine and serpentine: implication for bioleaching of high-magnesium nickel sulfide ore at elevated pH. Int. J. Miner. Metallurg. Mater. 26 (9), 1069–1079. https://doi.org/10.1007/s12613-019-1823-8.

Thom, James, Dipple, Greg, Power, Ian, Harrison, Anna, 2013. Chrysotile dissolution rates: Implications for carbon sequestration. Appl. Geochem. 35, 244–254. https://doi.org/10.1016/j.apgeochem.2013.04.016.

Tosca, N. J ., & Masterson, A. L. (2014). Chemical controls on incipient Mg-silicate crystallization at 25°C: Implications for early and late diagenesis. Clay Minerals, 49 (2), 165–194. https://doi.org/10.1180/claymin.2014.049.2.03.

Turvey, Connor Charles, 2018. Formation, Reaction Rates and Stability of Hydrotalcite-Group Minerals : Applications for Carbon Mineralization.

Turvey, Connor C., Wilson, S.A., Hamilton, J.L., Tait, A.W., McCutcheon, J., Beinlich, A., Southam, G., 2018. Hydrotalcites and hydrated Mg-carbonates as carbon sinks in serpentinite mineral wastes from the Woodsreef chrysotile mine, New South Wales, Australia: controls on carbonate mineralogy and efficiency of CO2 air capture in mine tailings. Int. J. Greenh. Gas Control 79, 38–60. https://doi.org/10.1016/j.ijggc.2018.09.015. October 2018.

Tutolo, B.M., Awolayo, A., Brown, C., 2021. Alkalinity generation constraints on basalt carbonation for carbon dioxide removal at the gigaton-per-year scale. Environ. Sci. Technol. 55 (17), 11906–11915. https://doi.org/10.1021/acs.est.1c02733.

Vance, D., Teagle, D.A.H., Foster, G.L., 2009. Variable Quaternary chemical weathering fluxes and imbalances in marine geochemical budgets. Nature 458 (7237), 493–496. https://doi.org/10.1038/nature07828.

Vermilyea, D.A., 1969. The dissolution of MgO and Mg(OH)2 in aqueous solutions. J. Electrochem. Soc. 116 (9), 1179–1183. https://doi.org/10.1149/1.2412273.

Vogeli, J., Reid, D.L., Becker, M., Broadhurst, J., Franzidis, J.P., 2011. Investigation of the potential for mineral carbonation of P.G.M. tailings in South Africa. Miner. Eng. 24 (12), 1348–1356. https://doi.org/10.1016/j.mineng.2011.07.005.

Wang, F., Dreisinger, D., Jarvis, M., Hitchins, T., 2019. Kinetics and mechanism of mineral carbonation of olivine for CO2 sequestration. Miner. Eng. 131, 185–197. https://doi.org/10.1016/j.mineng.2018.11.024. October 2018.

Washbourne, C.L., Renforth, P., Manning, D.A.C., 2012. Investigating carbonate formation in urban soils as a method for capture and storage of atmospheric carbon. Sci. Total Environ. 431, 166–175. https://doi.org/10.1016/j.scitotenv.2012.05.037.

White, A.F., Brantley, S.L., 2003. The effect of time on the weathering of silicate minerals: why do weathering rates differ in the laboratory and field? Chem. Geol. 202 (3–4), 479–506. https://doi.org/10.1016/j.chemgeo.2003.03.001.

Wieland, E., Stumm, W., 1992. Dissolution kinetics of kaolinite in acidic aqueous solutions at 25°C. Geochem. Cosmochim. Acta 56 (9), 3339–3355. https://doi.org/10.1016/0016-7037(92)90382-S.

Wilson, S., Raudsepp, M., Dipple, G., 2009. Quantifying carbon fixation in trace minerals from processed kimberlite: a comparative study of quantitative methods using x-ray powder diffraction data with applications to the Diavik Diamond Mine, Northwest Territories, Canada. Appl. Geochem. 24 (12), 2312–2331. https://doi.org/10.1016/j.apgeochem.2009.09.018.

Wilson, Siobhan, Barker, Shaun, Dipple, Greg, Atudorei, Viorel, 2010. Isotopic disequilibrium during uptake of atmospheric CO2 into mine process waters: implications for CO2 sequestration. Environ. Sci. Technol. 44, 9522–9529. https://doi.org/10.1021/es1021125.

Wilson, Siobhan, Harrison, Anna, Dipple, Greg, Power, Ian, Barker, Shaun, Mayer, K., Fallon, Stewart, Raudsepp, Mati, Southam, Gordon, 2014. Offsetting of CO2 emissions by air capture in mine tailings at the Mount Keith Nickel Mine, Western Australia: rates, controls and prospects for carbon-neutral mining. Int. J. Greenh. Gas Control 25, 121–140. https://doi.org/10.1016/j.ijggc.2014.04.002.

Woodall, C.M., Lu, X., Dipple, G., Wilcox, J., 2021. Carbon mineralization with north american pgm mine tailings—characterization and reactivity analysis. Minerals 11 (8), 1–16. https://doi.org/10.3390/min11080844.

Zevenhoven, R., Teir, S., Eloneva, S., 2008. Heat optimization of a staged gas-solid mineral carbonation process for long-term CO2 storage. Energy 33 (2), 362–370. https://doi.org/10.1016/j.energy.2007.11.005.

Zinder, B., Furrer, G., Stumm, W., 1986. The coordination chemistry of weathering: II. Dissolution of Fe(III) oxides. Geochem. Cosmochim. Acta 50 (9), 1861–1869. https://doi.org/10.1016/0016-7037(86)90244-9.